How to cite: *Angew. Chem. Int. Ed.* **2022,** *61,* e202201563
International Edition: doi.org/10.1002/anie.202201563
German Edition: doi.org/10.1002/ange.202201563

Antibacterial Coating

A Metal-Ion-Incorporated Mussel-Inspired Poly(Vinyl Alcohol)-Based Polymer Coating Offers Improved Antibacterial Activity and Cellular Mechanoresponse Manipulation

Lingyan Gao[+], Yong Hou[+], Haojie Wang, Mingjun Li,* Linjie Ma, Zhiqin Chu, Ievgen S. Donskyi, and Rainer Haag**

Abstract: Cobalt (Co^{II}) ions have been an attractive candidate for the biomedical modification of orthopedic implants for decades. However, limited research has been performed into how immobilized Co^{II} ions affect the physical properties of implant devices and how these changes regulate cellular behavior. In this study we modified biocompatible poly(vinyl alcohol) with terpyridine and catechol groups (PVA-TP-CA) to create a stable surface coating in which bioactive metal ions could be anchored, endowing the coating with improved broad-spectrum antibacterial activity against *Escherichia coli* and *Staphylococcus aureus*, as well as enhanced surface stiffness and cellular mechanoresponse manipulation. Strengthened by the addition of these metal ions, the coating elicited enhanced mechanosensing from adjacent cells, facilitating cell adhesion, spreading, proliferation, and osteogenic differentiation on the surface coating. This dual-functional PVA-TP-CA/Co surface coating offers a promising approach for improving clinical implantation outcomes.

Introduction

Rapidly increasing research toward the exploration and production of implantable devices for clinical treatment has revealed an urgent need for materials with specific chemical and physical properties that can enhance their biological functions.[1] Introducing implants into lesion sites not only provides mechanical support and adhesion sites for cell adhesion and migration, but also presents various biochemical cues (soluble and insoluble growth factors, cell-adhesive ligands and cell-to-cell contact) and biophysical cues (stiffness, topography and porosity) that together regulate cell response in the areas of spreading, differentiation, self-renewal and migration.[2] Therefore, designing a biointerface with controllable biochemical and biophysical properties that manipulate cellular functions presents an attractive research target in tissue engineering. Furthermore, bacterial contamination on implantable surfaces has emerged as a severe post-implantation problem in current-stage clinical applications, which can lead to orthopedic complications and even trauma, with their attending high rates of morbidity and mortality.[3] Much attention has been directed toward developing implantable materials whose antibacterial activity arises from surface decoration with antibacterial agents, an approach that may decrease the risk of implant-based infections and prevent postsurgical infections.[4]

Osteointegration is an important factor in the success of clinical implantation. Various bioactive agents, such as peptide, enzymes and growth factors, have been used in biomaterials to enable osteointegration.[4] However, maintaining high bioactivity of these agents during fabrication has proven challenging. Cobalt (Co^{II}) ions have recently emerged as an attractive candidate for the biomedical modification of implants, due to their remarkable biological activity and their stability during fabrication.[6] In addition to their excellent antibacterial activity,[6a,e] numerous studies have revealed that Co^{II} ions at appropriate concentrations contribute positively to the regulation of angiogenesis in

[*] Assoc. Prof. Dr. L. Gao,[+] H. Wang
Key Laboratory of Synthetic and Natural Functional Molecule Chemistry of the Ministry of Education, College of Chemistry & Materials Science,
Northwest University, 710069 Xi'an (China)
E-mail: gaolingyan@nwu.edu.cn

Dr. Y. Hou,[+] Dr. M. Li, Dr. I. S. Donskyi, Prof. Dr. R. Haag
Institut für Chemie und Biochemie, Freie Universität Berlin,
Takustrasse 3, 14195 Berlin (Germany)
E-mail: haag@chemie.fu-berlin.de

Dr. M. Li
School of Health Sciences and Biomedical Engineering,
Hebei University of Technology,
300130 Tianjin (China)
E-mail: limingjun0000@126.com

Dr. Y. Hou,[+] L. Ma, Z. Chu
Department of Electrical and Electronic Engineering,
The University of Hong Kong,
Pokfulam Road, Hong Kong (Hong Kong)

[+] These authors contributed equally to this work.

bone formation.[6b–f,7] Co^{II} ions in implants have shown an ability to stabilize the hypoxia-inducible factors (HIFs) and initiate a cascade of proangiogenic factors including vascular endothelial growth factor (VEGF), resulting in enhanced vessel formation and coupling of osteogenesis and angiogenesis.[6b] Compared with other biological methods like bone grafting with a vascular bone flap, gene therapy, and application of expensive recombinant VEGF proteins, the cobalt-induced vascularized bone regeneration platform is much easier to operate and less costly to fabricate.[8]

To date, studies in this area have focused on the cellular effects of Co^{II} ions or debris released from cobalt-based biomaterials in the culture environment.[6,7] However, the biological activity of Co^{II} ions is highly dose-dependent. For instance, high levels of Co^{II} ions in the body may cause an excessive inflammatory reaction, osteolysis, and consequently failure of the implant.[7c] Recently, it was found that the surface topographic features of implanted devices, for instance, substrate stiffness or surface roughness, can dramatically influence cellular functions.[9] However, to the best of our knowledge, limited research has been performed into how surface-immobilized metal ions affect the physical properties of the implant devices and how these changes influence cellular behavior.[10] Therefore, it would be significant to study the immobilized metal ions' influence on the implant surface, with an eye toward the resultant surface physical properties and tissue engineering implications.

With these aims in mind, we designed and synthesized biocompatible poly(vinyl alcohol) (PVA) modified with terpyridine (TP) and catechol (CA) groups to afford a new polymer, PVA-TP-CA (Scheme 1). Because of the strong adhesive activity of catechol on organic and inorganic surfaces,[11] we were able to efficiently construct polymer PVA-TP-CA as an initial polymeric layer on a silicon wafer surface. The strong coordination interactions between metal ions and ligand (TP and residual oxidative CA) have offered a well-traveled path to fabricate versatile metal-incorporated materials.[12] In this study, the Co^{II} ions immobilized in the surface coating changed the physical properties of the material surface to a remarkable degree through the formation of metal–ligand complexes. The modified surface coating with enhanced surface stiffness not only showed good biocompatibility alongside excellent and durable antibacterial activity toward gram-negative *Escherichia coli* (*E. coli*, ATCC25922) and *Staphylococcus aureus* (*S. aureus*, ATCC25923), but also promoted the adhesion, spreading, proliferation and osteogenic differentiation of human mesenchymal stem cells (hMSCs) on the surface. This antibacterial surface coating provides a favorable platform, with specific cell adhesion and osteogenesis properties, that can be further developed into a multifunctional implantable device.

Results and Discussion

PVA, an FDA-approved biocompatible polymer, can be easily functionalized with different moieties through the

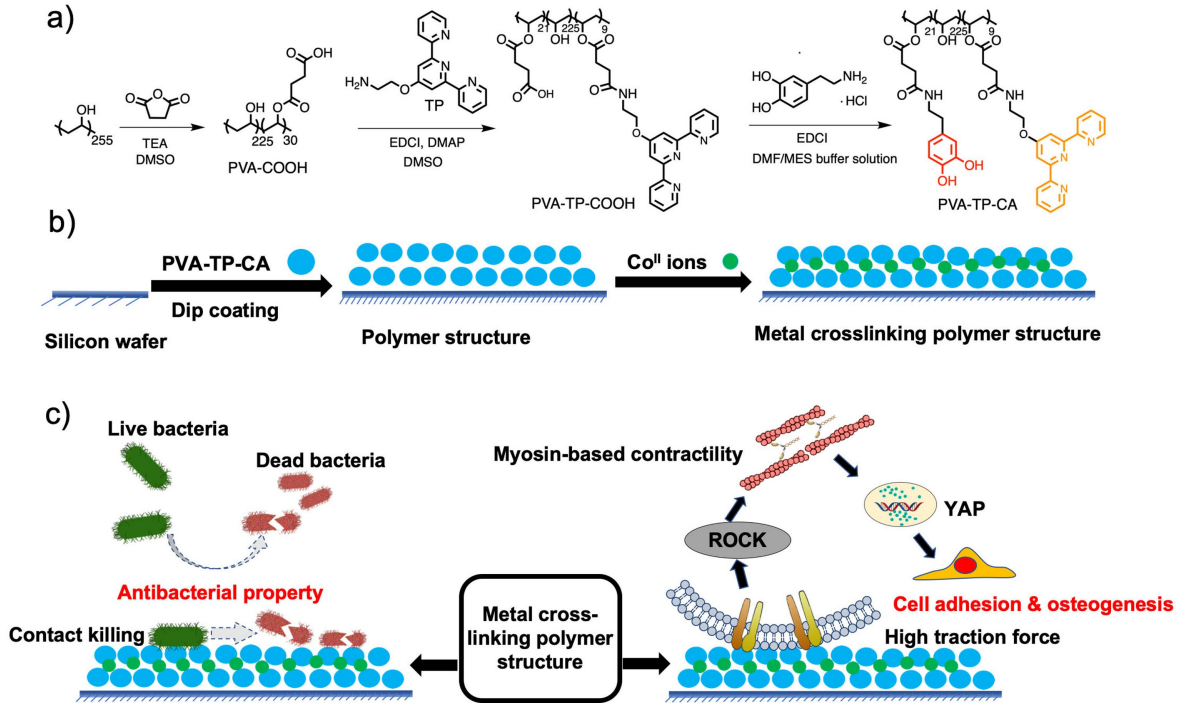

Scheme 1. a) The synthetic route for the polymer PVA-TP-CA, b) schematic representation of the preparation of PVA-TP-CA surface coatings encapsulated with Co^{II} ions and c) schematic illustration of the role that metal ions in PVA-TP-CA polymer coatings play in antibacterial activity and in regulating cell adhesion and fate determination. On one hand, metal ions on the polymeric surface coating realize antibacterial ability via contact killing of bacteria, while on the other hand, cells sense substrate stiffness via the focal adhesion-ROCK-actomyosin-YAP/TAZ signaling pathway.

OH groups on the polymer backbone. In this work, 30 OH groups on the polymer chain were changed to carboxyl groups. Then, 9 carboxyl groups were conjugated with 2-([2,2′:6′,2″-terpyridin]-4′-yloxy)ethan-1-amine (TP) through an amine coupling reaction to obtain a new polymer, PVA-TP-COOH. Subsequently, the remaining carboxyl groups on polymer PVA-TP-COOH were reacted with dopamine to afford the final polymer, PVA-TP-CA (Scheme 1).

As dopamine can self-polymerize to form surface-adherent polydopamine films on a wide range of organic and inorganic materials, the polymer PVA-TP-CA with catechol groups was able to spontaneously and rapidly form an initial polymeric layer on a silicon wafer via a simple dip-coating strategy at room temperature. Specifically, we simply immersed silicon wafers in a dilute aqueous solution of polymer PVA-TP-CA (3 mg ml^{-1}), then adjusted the pH to alkaline conditions by the addition of MOPs buffer (pH 8.5). The catechol groups on the polymer underwent oxidative polymerization and generated aggregates that were resistant to common organic solvents, resulting in the formation of an adherent polymer film on the silicon wafer surface. Different coating times (2, 4, 8 and 12 h) were investigated to observe the thickness of the polymeric layers. The thickness ranged from nanometer to micrometer scales as the incubation time increased from 2 to 12 h, a finding confirmed by ellipsometry. For the surface coatings with 2, 4 or 8 h incubation time, the thickness gradually increased from average 6 nm, to 11 nm, to 22 nm, respectively; the average contact angles accordingly increased from ca. 55° to 75° and 80°, respectively. It was noted that the surface coatings fabricated within 8 h were stable in aqueous solutions for as long as 4 weeks as determined by ellipsometry, while the micrometer-range layer under 12 h incubation time showed deformation after immersion in solution for 24 h. This deformation might be attributed to the significantly increased micrometer-scale thickness of the coating, which would induce a higher swelling capacity and lower stability, making ductile fracture of the coating much easier. Taking consideration of ease of preparation and stability of the surface coating for further biological applications, we used a coating time of 4 h in fabricating the PVA-TP-CA surface coating.

Subsequently, the polymeric layer under 4 h incubation time was closely investigated by scanning electron microscopy (SEM), X-ray photoelectron spectroscopy (XPS), and contact angle measurement. From the SEM image (Figure 1a), we observed that a dense phase-separated polymer coating was formed on the silicon wafer. The XPS result shown in Figure 1b demonstrated the presence of carbon, nitrogen and oxygen in the prepared surface coating, which confirmed the formation of the PVA-TP-CA surface coating. The surface coating was then immersed in a $CoCl_2$ solution (2 mg mL^{-1}). Due to the chelation between metal

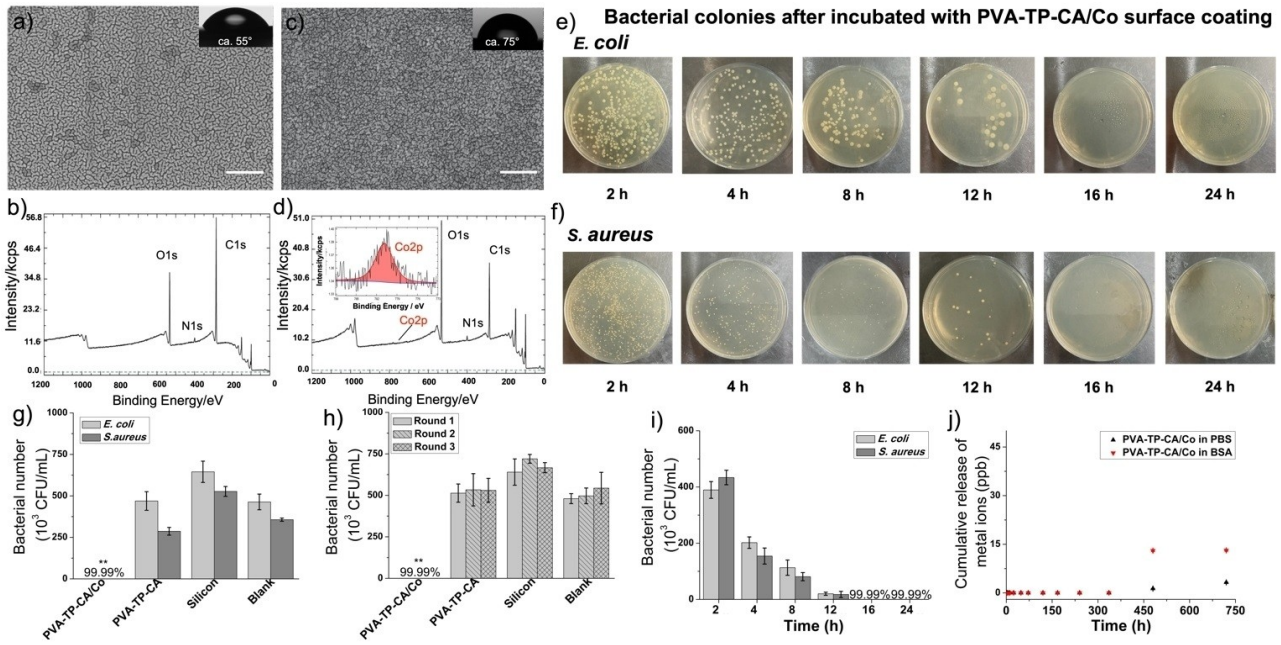

Figure 1. SEM images of a) PVA-TP-CA surface coating and c) PVA-TP-CA/Co surface coating c). Scale bar, 500 nm. Insets in a) and c) represent the respective static water contact angles of the PVA-TP-CA and PVA-TP-CA/Co surface coatings. XPS spectra of b) PVA-TP-CA surface coating and d) PVA-TP-CA/Co surface coating. Inset in d) is the enlarged XPS spectrum for Co2p. Time-dependent antibacterial activity of PVA-TP-CA/Co surface coating against e) *E. coli* and f) *S. aureus*. g) Bacterial numbers after incubation with PVA-TP-CA/Co and PVA-TP-CA surface coatings and bare silicon wafer in solution of *E. coli* and *S. aureus*. h) Bacterial numbers for three rounds of continuous antibacterial tests against *E. coli*. i) Bacterial numbers after incubation with PVA-TP-CA/Co surface coatings with different incubation times against *E. coli* and *S. aureus* suspensions. j) Cumulative release profile of Co^{II} ions from PVA-TP-CA/Co surface coatings immersed in PBS or buffered BSA solution. Data are presented as the mean ± SD, $n = 3$. Statistically significant differences at the same period are indicated by $^{**}p < 0.01$ compared with blank control.

ions and ligands (TP and residual oxidative CA) on the polymer backbone, Co^{II} ions were stabilized in the surface coating networks, as confirmed by the UV/Vis spectroscopic studies (Figure S4). The morphology of the new polymer coating (PVA-TP-CA/Co) was more compact (Figure 1c) than PVA-TP-CA. The contact angle of the new surface coating increased from 55° (PVA-TP-CA) to 75° (PVA-TP-CA/Co) (inset pictures in Figure 1a,c). The XPS result shown in Figure 1d gave direct evidence for the existence of Co^{II} ions in the surface coating: a peak at 780.0 eV could be observed in the spectrum, corresponding to Co^{II} ions. Furthermore, the enlarged, highly resolved Co2p spectrum (Figure 1d) revealed that the atomic percentage of the Co^{II} ions was around 0.1 %.

It is well-known that Co^{II} ions demonstrate antibacterial activity in solution. Therefore, we treated the PVA-TP-CA/Co surface coating with representative gram-negative *E. coli* and gram-positive *S. aureus*, to examine whether the antibacterial activity of Co^{II} ions persisted in the metal-terpyridine complexes. The PVA-TP-CA/Co surface coating on silicon wafer showed strong antibacterial activity, with more than 99.99 % bacterial reduction efficiency (Figure 1g). By contrast, the bare silicon wafer and PVA-TP-CA surface coating showed no antibacterial activity, indicating that the Co^{II} ions were responsible for the bacterial reduction by the PVA-TP-CA/Co surface coating. Furthermore, the antibacterial effects of the PVA-TP-CA/Co surface coating against *E. coli* and *S. aureus* are time-dependent (Figure 1e,f,i). After 8 h of incubation, about 71 % of *E. coli* and 81 % of *S. aureus.* were killed by PVA-TP-CA/Co surface coatings. After 12 h, around 94 % of *E. coli* and 96 % of *S. aureus.* had been destroyed, and after 16 h of incubation almost 99.9 % of both types of bacteria were dead. The corresponding bacterial colonies cocultured with PVA-TP-CA/Co surface coatings with different times are shown in Figure 1e,f. Notably, our PVA-TP-CA/Co surface coating can also be constructed on the TC4 titanium alloy, which is widely used in the clinical bone regeneration. The PVA-TP-CA/Co surface coatings on TC4 titanium alloys showed excellent antibacterial activity against *E. coli* and *S. aureus*, killing 99.99 % bacteria in solution in 24 h of incubation (Figure S5) and suggesting compatibility of PVA-TP-CA/Co surface coatings with a wide range of different substrates.

The addition of Co^{II} ions imparted excellent antibacterial properties to the PVA-TP-CA/Co surface coating. However, the antibacterial mechanism of this coating is unclear. In accordance with the reported literature,[13] we proposed two candidates: a) the release of antibacterial Co^{II} ions from the surface coating; and b) the continuous and effective contact between bacteria and the coating. To understand the antibacterial activity of the Co^{II} ions in the surface coating, we carried out inductively coupled plasma mass spectrometry (ICP-MS) to investigate whether the Co^{II} ions could be released from the coating.

Since the release of Co^{II} ions from the surface coating may be induced by interaction between the metal ions and the bacteria's metalloproteins,[14] we conducted the release study by incubating the polymer coatings with a model protein, bovine serum albumin (BSA). This protein is widely recognized to show affinities towards a multitude of metal ions, including Co^{II}, Zn^{II}, Fe^{II}, Cu^{II}, Ni^{II}, and Mg^{II}.[15] The use of BSA can also prevent metal ions (derived from the leakage of metalloproteins from destroyed bacteria) from interfering in the ICP-MS measurement.[16]

PVA-TP-CA/Co surface coatings were immersed in phosphate buffer (PBS) or buffered BSA solution (3.5 %, w/v) for various time periods: 2 h, 4 h, 8 h, 12 h, 24 h, 2 d, 3 d, 5 d, 7 d, 10 d, 14 d, 20 d, and 30 d. The ICP-MS measurements on day 14 revealed that Co^{II} ions in the PVA-TP-CA surface coating remained quite stable in PBS in the absence and presence of BSA: no significant Co^{II} ions could be detected (<1 ppb) from the leachate (Figure 1j). Over the next 16 days, the Co^{II} ions remained stable in the PBS solutions, showing a slight increase to 3.2 ppb by day 30. Meanwhile, after 30 d in the BSA solution, the released Co^{II} ions reached a concentration of 13.1 ppb, representing a tiny number of ions at a level of nontoxic to bacteria (Figure S6) and human osteoblast-like cells[17] (Figure 1j). This result might be ascribed to the long incubation time and the weak binding competition from BSA ($\log K_{BSA\text{-}Co^{II}} \approx 4.19$[15b] vs. $\log \beta_{terpyridine\text{-}Co^{II}} > 16$[12]).

In other words, due to the strong binding affinity of Co^{II} ions for the PVA-TP-CA surface coating and the low affinity of Co^{II} ions for BSA, the embedded Co^{II} ions were quite stable for 30 days not only in PBS but also in the presence of protein. As BSA was used to mimic the interaction of bacteria and the surface coating, we supposed that the incorporated Co^{II} ions in the coating were also stable during the incubation with bacterial suspension. It is therefore possible that the antibacterial activity of the PVA-TP-CA/Co surface coating can be ascribed to continuous and effective contact between bacteria and the coating (Scheme 1c), which may damage the cell wall or reduce the cell membrane integrity, leading finally to cell death. Martin et al. reported similar results, finding that direct contact with a cobalt-incorporated surface resulted in a strong antibacterial effect.[13b] In addition, as the incorporated Co^{II} ions were quite stable, the antibacterial activity of the PVA-TP-CA/Co surface coating could be maintained as the sample underwent three rounds of a continuous antibacterial test against *E. coli* (Figure 1h) and *S. aureus.* (Figure S7), revealing that the PVA-TP-CA/Co surface coating can act as a durable antibacterial material. These results suggest that the coordination interactions between ligands on the polymer backbone and Co^{II} ions were stable enough to preserve the bioactive Co^{II} ions in the surface coating networks under approximately physiological conditions; this stability is crucial in determining the coating's in vitro and in vivo bioactivity.

We further evaluated the PVA-TP-CA/Co surface coating for potential application in tissue engineering. We first performed a 3-(4,5-dimethyl-2-thiazolyl)-2,5-diphenyltetrazolium bromide (MTT) assay to evaluate the coating's biocompatibility with the hMSCs. The cells' absorbance at 570 nm (OD_{570}) after 24 and 72 h cultured in the medium revealed that they maintained a relatively high viability and

were able to adhere, spread, and proliferate well on the coating (Figure 2d). The metabolic activities of the cells were comparable on a bare silicon wafer and on the PVA-TP-CA/Co surface coating. In addition, after 24 h the level of metabolic activity on the PVA-TP-CA/Co surface coating was significantly higher than on the PVA-TP-CA surface coating. Furthermore, after a longer incubation time of 72 h on these surfaces, the cells still showed strong proliferation and comparable levels of metabolic activity between the two surface coatings. These results demonstrated that the PVA-TP-CA/Co surface coating was biocompatible with the hMSCs.

We subsequently investigated early-stage cell adhesion in detail by culturing the hMSCs on the coatings for 4 h. As shown in Figures 2a, e, and S8, cells on the PVA-TP-CA/Co surface coating displayed the largest spreading area (2833 μm^2) and the highest aspect ratio (3.3). More elongated cells with denser actin fibers were observed on the PVA-TP-CA/Co surface coating than on the Co^{II} ion-free coatings (Figure 2a, b). This result demonstrates that the introduction of Co^{II} ions dramatically enhanced cell adhesion on the PVA-TP-CA/Co coating. As the ICP-MS measurement revealed, no Co^{II} ions were released from the PVA-TP-CA/Co surface coating, and therefore the Co^{II} ions could not have affected cell adhesion through the chemical mechanism wherein free Co^{II} ions cross the cytoplasmic membrane, bind with DNA and regulate downstream gene and protein expression. The Co^{II} ions encapsulated in the PVA-TP-CA/Co surface coating must therefore have influenced the biosystem in a different way.

Normal tissue cells must adhere to a solid to realize their functions. The rigidity of the solid biointerface, also referred to as stiffness or elasticity, can be sensed by cells and can impact their behavior. As reported in the literature, Co^{II} ions can bind with terpyridine in water at a constant ratio of 1:2 ($\log\beta_{terpyridine\text{-}Co^{II}} > 16$).[12] The strong coordination between the Co^{II} ions and terpyridine groups in the polymer PVA-TP-CA could enhance the mechanical properties of the coatings, possibly providing enough traction force for cell adhesion and spreading. As a proof of concept, we used Fe^{II} ions and Zn^{II} ions, two other coordinate metal ions for terpyridine, as reference metal ions. Fe^{II} ions can also form relatively stable metal-terpyridine complexes (constant ratio of 1:2, $\log\beta_{terpyridine\text{-}Fe^{II}} > 16$), while Zn^{II} ions will form weaker mono-complexes when the metal-ion/terpyridine ratio is higher than 0.5 ($\log K_{terpyridine\text{-}Zn^{II}} \approx 6.0$).[12] By adding excess Co^{II}, Fe^{II} or Zn^{II} ions in the PVA-TP-CA surface coating, we achieved PVA-TP-CA surfaces with different mechanical properties. We performed the surface mechanical study using atomic force microscopy (AFM).

As expected, the mechanical strength of the PVA-TP-CA/Co coatings was enhanced by the addition of the metal ions. The Young's modulus of PVA-TP-CA/Co is 6.3 kPa, a value that is 1.49-fold, 6.02-fold, and 11.18-fold higher than those of PVA-TP-CA/Fe, PVA-TP-CA/Zn, and blank control, respectively (Figure 3c). In addition, these three

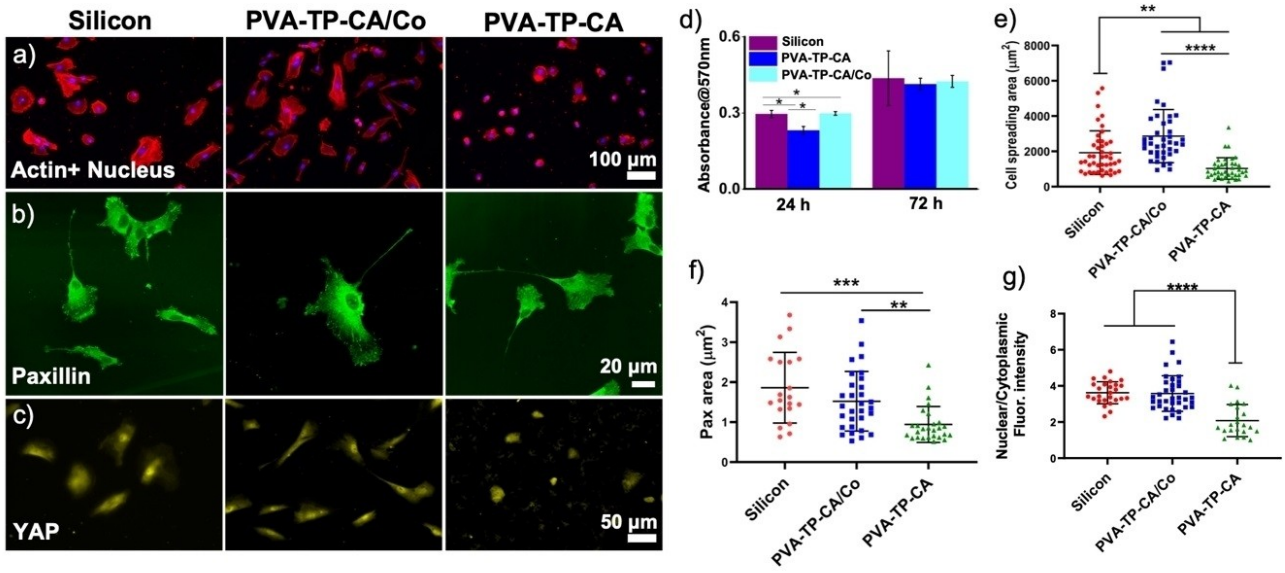

Figure 2. PVA-based polymer coatings embedded with Co^{II} ions regulate cell adhesion and proliferation. a) Morphology of hMSCs after 4 h of culture on different surfaces. The cells' actin fibers were stained with phalloidin (red) and their nuclei were stained with 4′, 6-diamidino-2-phenylindole (DAPI, blue). b) Surface stiffness modulates the cells' focal adhesion (FA) formation on different surfaces. Cells were stained with anti-paxillin (green). c) Representative fluorescence images of hMSCs stained with anti-yes-associated protein (YAP, cyan) on different surfaces. d) Metabolic activities of hMSCs on different surfaces after 24 and 72 h cultured in the medium. e–g) Quantification of cell area, FA area and YAP nuclear/cytoplasmic ratio of hMSCs on different surfaces after 4 h of culture. Mean values and standard deviations from 30 to 40 cells are presented. P-values < 0.05 were considered statistically significant ($^{*}p < 0.05$, $^{**}p < 0.01$, $^{***}p < 0.001$).

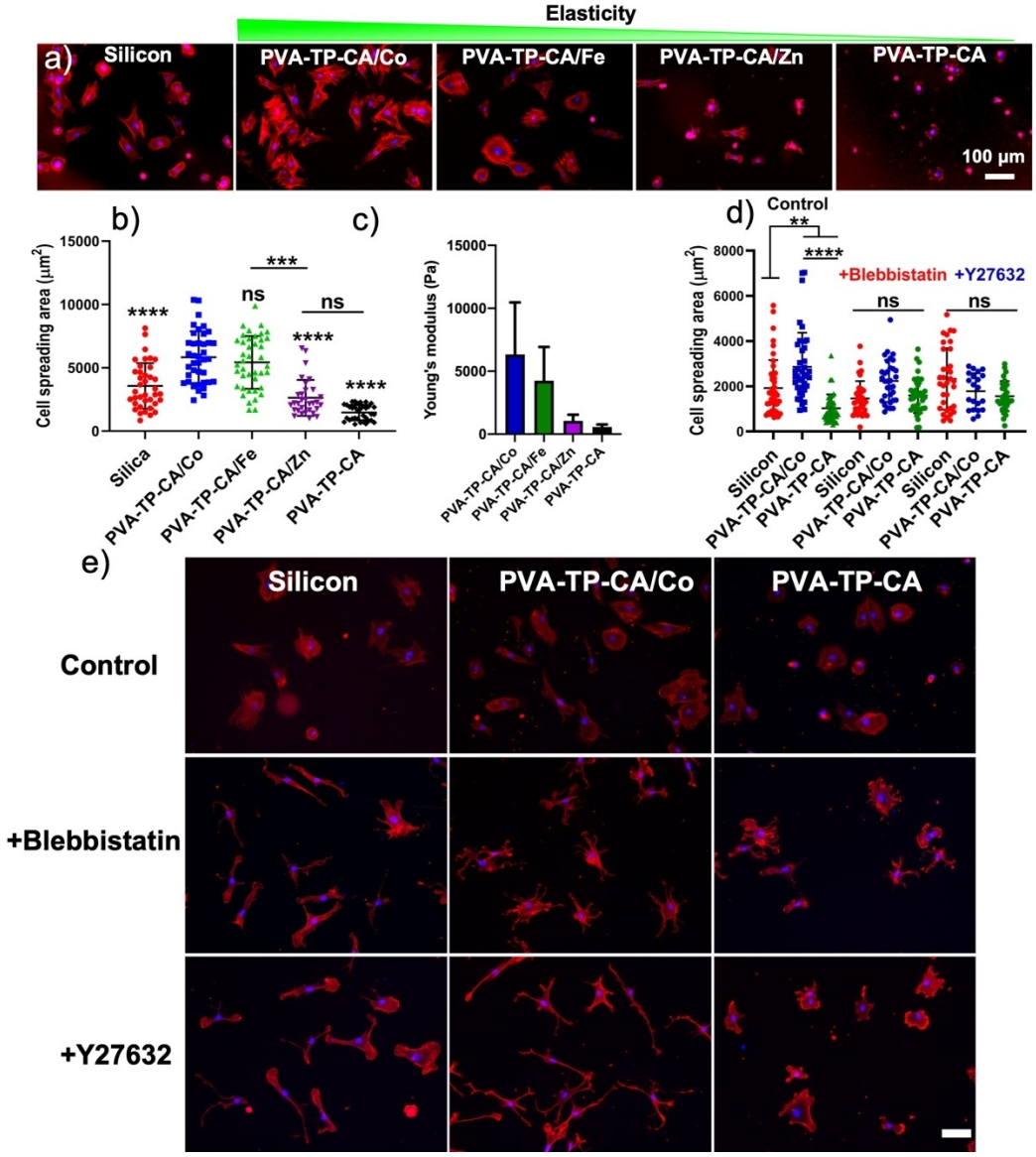

Figure 3. Cellular response to PVA-TP-CA coatings treated with different metal ions. a) The morphologies of hMSCs after 4 h of culture on different surfaces. The cell actin fibers were stained with phalloidin (red) and the cell nuclei were stained with DAPI (blue). b) Spreading area of cells on different surfaces. c) Young's modulus of PVA-TP-CA coatings treated with different metal ions. d) Cell spread areas on different surfaces after being treated with Y27632 or blebbistatin for 24 h. e) Representative images of F-actin-stained cells after being treated with control, blebbistatin and Y27632 on bare silicon wafer (left column), PVA-TP-CA/Co surface coating (middle column) and PVA-TP-CA surface coating (right column). Scale bar, 100 μm. P-values <0.05 were considered statistically significant (** $p<0.01$, *** $p<0.001$, **** $p<0.0001$).

metal-treated PVA-TP-CA coatings revealed no clear difference in surface physical properties like morphology, hydrophilicity and hydrophobicity (Figure S3). After seeding the cells on the metal-treated PVA-TP-CA coatings for 4 h, we found that these coatings promoted the spreading of cells as compared with blank polymer coatings. In addition, the PVA-TP-CA/Fe surface coating promoted cell adhesion more strongly than the metal-free coatings. No significant difference was found between the cell spreading areas on the PVA-TP-CA/Co and PVA-TP-CA/Fe surfaces (Figure 3a,b), a result that may be attributable to their comparable mechanical properties (Figure 3c). On the other hand, the cells on the PVA-TP-CA/Zn surface coating with lower Young's moduli showed limited cell adhesion, exhibiting no significant difference to cells on the PVA-TP-CA surface (Figure 3a,b). Taken together, these data revealed that the mechanical strength of the metal-incorporated polymer coating played a central role in regulating cell functions. The stronger the metal-terpyridine coordination, the stiffer the coating; and the stiffer the coating, the more conducive it is to cell adhesion.

The mechanical properties of extracellular matrix (ECM) vary, and cells can agilely detect the subtle mechanical strength differences within the ECM through integrin-based focal adhesions (FAs). The force-sensing molecules in FAs can convert physical signals from the

ECM to intracellular biochemical signals to induce cellular contractility through cytoskeletons. The cells contract their actomyosin cytoskeleton, generating mechanical forces at the sites of adhesion in order to maintain homeostasis. Therefore, the expression and arrangement of FAs can directly reflect cell mechanics. We therefore stained paxillin at FAs to investigate whether the enhanced substrate mechanics contributed to the assembly of the cells' FAs. We observed larger FA areas (1.47 μm^2) on the stiffer PVA-TP-CA/Co surface coating; this result is 1.58-fold the size of the area measured on the PVA-TP-CA surface coating (Figure 2b, f). These results are consistent with the observed cell spreading, suggesting that the best cell adhesion occurs on Co^{II} ion-treated PVA-TP-CA surface coatings.

Furthermore, in a process known as mechanotransduction, the extracellular mechanical cues can be transduced through FAs to the cell nucleus to further regulate downstream signaling pathways and protein expression.[18] Yes-associated protein (YAP) has been identified as a transmembrane sensor of the structural and mechanical features of the cell microenvironment.[19] The hMSCs' adhesion and differentiation have been shown to be positively correlated with YAP activity.[9d] As expected, the YAP nuclear localization of cells on the stiffer PVA-TP-CA/Co surface coating and bare silicon showed brighter nuclear YAP fluorescence.

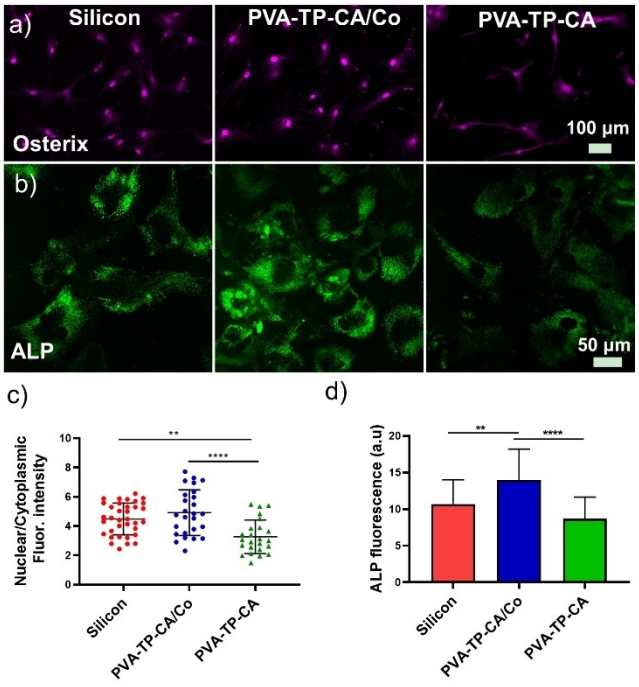

Figure 4. a) Representative images of osterix staining of hMSCs cultured on different surfaces after 5 days. b) Representative images of ALP staining of hMSCs cultured on different surfaces after 14 days. c, d) Quantification of osterix expression and ALP activity of hMSCs on different surface coatings after 5 and 14 days of induction, respectively. Mean values and standard deviations from 30 to 40 cells are presented. P-values < 0.05 were considered statistically significant (** $p < 0.01$, **** $p < 0.0001$).

In contrast, the fluorescence signaling of YAP in cells on the softer PVA-TP-CA coating localized homogeneously throughout the whole cell body due to the lack of cellular contractility (Figure 2c, g).

To further confirm the role of actomyosin-based contractility in the substrate mechanics sensing, we treated cells on all coatings with the myosin II inhibitor blebbistatin and the Rock inhibitor Y27632. The cell spread areas on the Co^{II} ion-treated and metal-free PVA-TP-CA coatings displayed obvious reductions after 4 h of culture, indicating the importance of actomyosin contractility in substrate-mechanics-induced cell adhesion and spreading (Figure 3d, e). From these results, we can infer that substrate mechanics enhancement signals induced by the Co^{II}-terpyridine coordination were sensed by focal adhesion proteins to activate ROCK signaling and modulate cellular contractility, which would facilitate the import of transcriptional regulator YAP into the nucleus and subsequently regulate downstream gene expression (Scheme 1c).

After the cell adhesion studies revealed the role of metal ions in PVA-TP-CA polymer coatings in antibacterial activity and regulating cell adhesion, we monitored in vitro osteogenic differentiation of hMSCs on the PVA-TP-CA/Co surface coating by the expression of osterix, an osteoblast-specific transcription factor, and the activity of alkaline phosphatase (ALP), an early marker for assessing osteoblastic metabolic activity. After 5 days of culture in osteogenic differentiation medium, nuclear osterix accumulation in cells on PVA-TP-CA/Co was 1.12-fold and 1.47-fold higher than on PVA-TP-CA and bare silicon surface respectively, indicating that the osteogenic differentiation was hindered on the metal-free coatings with lower mechanics (Figure 4a, c). ALP staining was performed at day 14 (Figure 4b, d). Compared with bare silicon wafer and the PVA-TP-CA surface coating, we observed a significantly higher level of ALP activity on the PVA-TP-CA/Co surface coating. Therefore, our novel PVA-TP-CA/Co surface coating, with its enhanced surface stiffness, enables specific cell adhesion, spreading, and osteogenesis and shows excellent and sustained antibacterial ability. These properties make it a promising candidate for implantable material coatings to promote new bone formation.

Conclusion

Using a simple dip-coating method via the integration of catechol chemistry and metal coordination chemistry, we fabricated a novel PVA-based antibacterial polymer coating, embedded with metal ions, that showed specific cell adhesion and osteogenesis properties. The PVA-based polymer, functionalized with terpyridine groups and catechol units, provided a biocompatible platform to efficiently anchor and stabilize bioactive Co^{II} ions. The immobilized Co^{II} ions on the surface coating endowed the material with sustained, powerful antibacterial activity towards gram-negative and gram-positive bacteria. The metal-ligand interactions enhanced the mechanical properties of the resulting polymeric surface coating to a remarkable degree. The

stronger mechanical stimulations were seen to dramatically promote the hMSCs' adhesion, spreading, proliferation and osteogenic differentiation. The newly developed PVA-TP-CA/Co surface coating described in this study, with its antibacterial and osteogenesis functions, offers a promising approach to improving outcomes in bone regeneration on implantable materials.

Acknowledgements

Lingyan Gao acknowledges the financial support from the National Natural Science Foundation of China (22101227), Natural Science Foundation of Shaanxi Province (2021JQ-433) and Young Talent Fund of University Association for Science and Technology in Shaanxi (20200603). Rainer Haag acknowledges the financial support from the SFB 765 of the Deutsche Forschungsgemeinschaft (DFG). Yong Hou and Mingjun Li acknowledge the financial support from China Scholarship Council (CSC). Zhiqin Chu acknowledges the financial support from the HKSAR Research Grants Council (RGC) General Research Fund (GRF; No. 14306117) and Early Career Scheme (ECS, No. 27202919). We thank the Core Facility BioSupraMol (Freie Universität Berlin, Germany) for the assistance in confocal microscopy measurements support and Benjamin Allen for his careful language polishing of the manuscript. Open Access funding enabled and organized by Projekt DEAL.

Conflict of Interest

The authors declare no conflict of interest.

Data Availability Statement

The data that support the findings of this study are available in the supplementary material of this article.

Keywords: Antibacterial Coating · Mechanotransduction · Metal Coordination · Osteogenesis · Supramolecular Chemistry

[1] a) J. Rychly, B. Nebe, *Cell Adh. Migr.* **2009**, *3*, 390–394; b) F. J. O'Brien, *Mater. Today* **2011**, *14*, 88–95; c) Q. Yu, Z. Wu, H. Chen, *Acta Biomater.* **2015**, *16*, 1–13.

[2] a) K. A. Myers, K. T. Applegate, G. Danuser, R. S. Fischer, C. M. Waterman, *J. Cell Biol.* **2011**, *192*, 321–334; b) A. Pathak, S. Kumar, *Proc. Natl. Acad. Sci. USA* **2012**, *109*, 10334–10339; c) M. Bao, J. Xie, W. T. S. Huck, *Adv. Sci.* **2018**, *5*, 1800448.

[3] a) G. Taubes, *Science* **2008**, *321*, 356–361; b) K. Bush, P. Courvalin, G. Dantas, J. Davies, B. Eisenstein, P. Huovinen, G. A. Jacoby, R. Kishony, B. N. Kreiswirth, E. Kutter, S. A. Lerner, S. Levy, K. Lewis, O. Lomovskaya, J. H. Miller, S. Mobashery, L. J. V. Piddock, S. Projan, C. M. Thomas, A. Tomasz, P. M. Tulkens, T. R. Walsh, J. D. Watson, J. Witkowski, W. Witte, G. Wright, P. Yeh, H. I. Zgurskaya, *Nat. Rev. Microbiol.* **2011**, *9*, 894–896.

[4] a) M. Krishnamoorthy, S. Hakobyan, M. Ramstedt, J. E. Gautrot, *Chem. Rev.* **2014**, *114*, 10976–11026; b) M. Benčina, T. Mavrič, I. Junkar, A. Bajt, A. Krajnović, K. Lakota, P. Žigon, S. Sodin-Šemrl, V. Kralj-Iglič, A. Iglič, in *Advances in Biomembranes and Lipid Self-Assembly, Vol. 28* (Eds.: A. Iglič, M. Rappolt, A. J. García-Sáez), Academic Press, San Diego, **2018**, pp. 115–165; c) Q. Zeng, Y. Zhu, B. Yu, Y. Sun, X. Ding, C. Xu, Y.-W. Wu, Z. Tang, F.-J. Xu, *Biomacromolecules* **2018**, *19*, 2805–2811.

[5] a) T. N. Vo, F. K. Kasper, A. G. Mikos, *Adv. Drug Delivery Rev.* **2012**, *64*, 1292–1309; b) C. von Wilmowsky, T. Moest, E. Nkenke, F. Stelzle, K. A. Schlegel, *Oral Maxillofac. Surg.* **2014**, *18*, 243–257; c) R. Quarto, P. Giannoni, in *Mesenchymal Stem Cells: Methods and Protocols* (Ed.: M. Gnecchi), Springer, New York, **2016**, pp. 21–33; d) I. Pountos, M. Panteli, A. Lampropoulos, E. Jones, G. M. Calori, P. V. Giannoudis, *BMC Med.* **2016**, *14*, 103; e) H. S. Alghamdi, *J. Funct. Biomater.* **2018**, *9*, 7.

[6] a) P.-K. O., C. M., Ć. S., *Acta Period. Technol.* **2004**, *35*, 231–238; b) C. Wu, Y. Zhou, W. Fan, P. Han, J. Chang, J. Yuen, M. Zhang, Y. Xiao, *Biomaterials* **2012**, *33*, 2076–2085; c) S. Kulanthaivel, U. Mishra, T. Agarwal, S. Giri, K. Pal, K. Pramanik, I. Banerjee, *Ceram. Int.* **2015**, *41*, 11323–11333; d) N. Ignjatović, Z. Ajduković, J. Rajković, S. Najman, D. Mihailović, D. Uskoković, *J. Bionic. Eng.* **2015**, *12*, 604–612; e) J. Zhou, L. Zhao, *Sci. Rep.* **2016**, *6*, 29069; f) I. D. Vlaicu, R. Olar, C. Maxim, M. C. Chifiriuc, C. Bleotu, N. Stănică, G. Vasile Scăeţeanu, C. Dulea, S. Avram, M. Badea, *Appl. Organomet. Chem.* **2019**, *33*, e4976.

[7] a) K. Glenske, P. Donkiewicz, A. Köwitsch, N. Milosevic-Oljaca, P. Rider, S. Rofall, J. Franke, O. Jung, R. Smeets, R. Schnettler, S. Wenisch, M. Barbeck, *Int. J. Mol. Sci.* **2018**, *19*, 826; b) A. Drynda, S. Drynda, J. Kekow, C. H. Lohmann, J. Bertrand, *Int. J. Mol. Sci.* **2018**, *19*, 3034; c) E. M. McCarthy, H. Floyd, O. Addison, Z. J. Zhang, P. G. Oppenheimer, L. M. Grover, *ACS Omega* **2018**, *3*, 10129–10138.

[8] a) T. Tanaka, I. Kojima, T. Ohse, J. R. Ingelfinger, S. Adler, T. Fujita, M. Nangaku, *Lab. Invest.* **2005**, *85*, 1292–1307; b) E. Quinlan, S. Partap, M. M. Azevedo, G. Jell, M. M. Stevens, F. J. O'Brien, *Biomaterials* **2015**, *52*, 358–366.

[9] a) D. E. Discher, P. Janmey, Y.-l. Wang, *Science* **2005**, *310*, 1139–1143; b) P. A. Janmey, C. A. McCulloch, *Annu. Rev. Biomed. Eng.* **2007**, *9*, 1–34; c) Y. Hou, L. Yu, W. Xie, L. C. Camacho, M. Zhang, Z. Chu, Q. Wei, R. Haag, *Nano Lett.* **2020**, *20*, 748–757; d) Y. Hou, W. Xie, L. Yu, L. C. Camacho, C. Nie, M. Zhang, R. Haag, Q. Wei, *Small* **2020**, *16*, 1905422.

[10] a) S. N. Nayab, F. H. Jones, I. Olsen, *Biomaterials* **2005**, *26*, 4717–4727; b) J.-W. Park, K.-B. Park, J.-Y. Suh, *Biomaterials* **2007**, *28*, 3306–3313; c) X.-B. Chen, Y.-C. Li, J. D. Plessis, P. D. Hodgson, C. E. Wen, *Acta Biomater.* **2009**, *5*, 1808–1820; d) J.-W. Park, Y.-J. Kim, J.-H. Jang, *Clin. Oral Implant. Res.* **2010**, *21*, 398–408; e) B. G. X. Zhang, D. E. Myers, G. G. Wallace, M. Brandt, P. F. M. Choong, *Int. J. Mol. Sci.* **2014**, *15*, 11878–11921.

[11] J. Sedó, J. Saiz-Poseu, F. Busqué, D. Ruiz-Molina, *Adv. Mater.* **2013**, *25*, 653–701.

[12] R. Shunmugam, G. J. Gabriel, K. A. Aamer, G. N. Tew, *Macromol. Rapid Commun.* **2010**, *31*, 784–793.

[13] a) M. Li, L. Nan, D. Xu, G. Ren, K. Yang, *J. Mater. Sci. Technol.* **2015**, *31*, 243–251; b) F. N. S. Raja, T. Worthington, M. A. Isaacs, L. Forto Chungong, B. Burke, O. Addison, R. A. Martin, *ACS Biomater. Sci. Eng.* **2019**, *5*, 283–293.

[14] K. J. Waldron, N. J. Robinson, *Nat. Rev. Microbiol.* **2009**, *7*, 25–35.

[15] a) X. Xu, L. Zhang, D. Shen, H. Wu, Q. Liu, *J. Fluoresc.* **2008**, *18*, 193–201; b) A. Singha Roy, D. R. Tripathy, A. Chatterjee, S. Dasgupta, *Spectrochim. Acta Part A* **2013**, *102*, 393–402; c) S.

Rudra, S. Dasmandal, C. Patra, A. Kundu, A. Mahapatra, *Spectrochim. Acta Part A* **2016**, *166*, 84–94.
[16] a) O. Y. Gavel, S. A. Bursakov, J. J. Calvete, G. N. George, J. J. G. Moura, I. Moura, *Biochemistry* **1998**, *37*, 16225–16232; b) L. D. Palmer, E. P. Skaar, *Annu. Rev. Genet.* **2016**, *50*, 67–91.
[17] L. Anissian, A. Stark, H. Dahlstrand, B. Granberg, V. Good, E. Bucht, *Acta Orthop. Scand.* **2002**, *73*, 369–374.
[18] K. A. Jansen, P. Atherton, C. Ballestrem, *Semin. Cell Dev. Biol.* **2017**, *71*, 75–83.
[19] C. K. K. Choi, Y. J. Xu, B. Wang, M. Zhu, L. Zhang, L. Bian, *Nano Lett.* **2015**, *15*, 6592–6600.

Manuscript received: January 28, 2022
Accepted manuscript online: February 18, 2022
Version of record online: March 24, 2022